High Speed Rotor Using SMBs Working in Vacuum Chamber

M. Komori, K. Hara, K. Asami, N. Sakai

Department of Applied Science for Integrated System Engineering, Kyushu Institute of Technology
1-1 Sensui, Tobata, Kitakyushu, Fukuoka 804-8550, Japan

This study is performed to apply superconducting magnetic bearings (SMBs) to a high speed turbine rotor. First, we analyze the system by using finite element method and design the structure whose vibrations are suppressed well. Then, we have made an experimental setup using the theoretical result. The experimental setup consists of two SMBs, a permanent magnet (PM) motor and a rotor with many turbine blades. We perform some experiments using this experimental setup in a vacuum chamber. In this paper, we discuss the dynamic characteristics of the spinning rotor with many turbine blades.

I. Introduction

Vacuum technology is necessary for semiconductor industry, medical industry and food industry [1]. The vacuum technology is also necessary for the new space industry and other advanced industries [2]. Turbo molecular pumps with high speed rotors are key technology for these industries. Turbo molecular pumps are usually composed of active magnetic bearings, a high speed rotor and its controllers. Thus, the mechanism is very precise and complicated, which leads to high prices. In this study, high critical temperature (T_c) superconducting magnetic bearings (SMBs) [3]-[5] are tried to apply to a high speed rotor for turbo molecular pump because of some merits.

II. SMB and Rotor Model

A. SMB

Fig.1 shows a schematic illustration of pinning effect in high T_c superconducting bulk. There are a lot of pinning centers composed of impurities in superconducting bulk. Magnetic fluxes are trapped and pinned at these pinning centers because of the low energy potential. SMBs are usually composed of superconducting bulks and PMs. Levitation force in SMB is produced using pinning effect.

M. Komori, K. Hara K. Asami and N. Sakai are with Department of Applied Science for Integrated System Engineering, Kyushu Institute of Technology, Fukuoka, 804-8550 Japan. Corresponding author: M. Komori (e-mail: komori_mk@yahoo.co.jp).

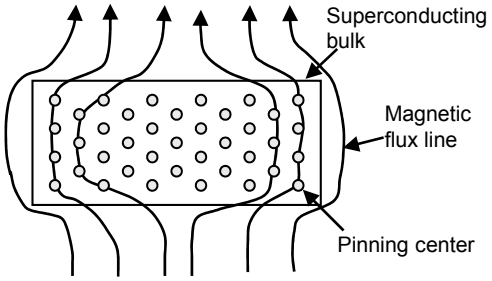

Fig. 1. Schematic illustration of pinning effect in high T_c superconducting bulk

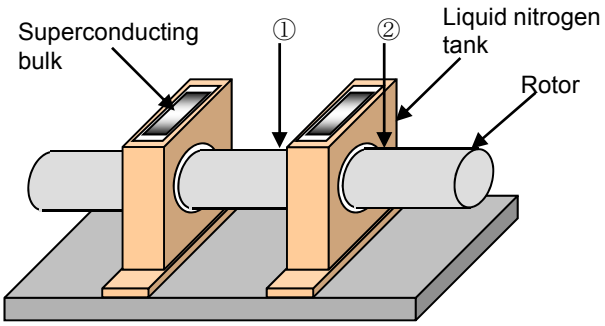

Fig. 2. Simple SMBs with a rotor. The SMB is composed of a doughnut-shaped superconducting bulk and four PMs.

Simple SMBs with a rotor are made as shown in Fig.2. The SMB is composed of a doughnut-shaped superconducting bulk $Dy_1Ba_2Cu_3O_X$ (OD48× ID25.6× 15 mm, J_c=3 ×108 A/m^2 at 77 K and 1.0 T) and four PMs. The PMs are neodymium (Nd) magnets (OD24 mm ×4.25 mm, surface magnetic flux density 0.26 T). The magnetic poles of the PMs are arranged with alternate polarities such as NS-SN-NS-SN. The superconducting bulks are cooled using liquid nitrogen (-196 °C).

Fig. 3 shows the experimental result of impulse response for the SMB without turbine blades. Thus,

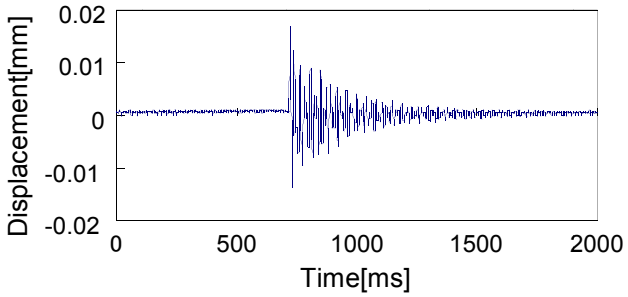

Fig. 3. Impulse response for the SMB without turbine blades.

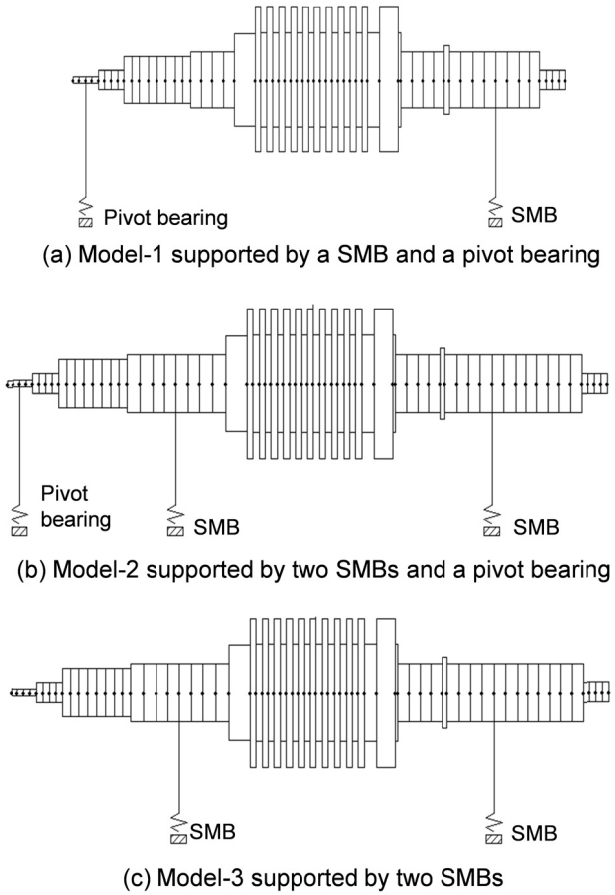

Fig. 4. Rotor models supported by two kinds of bearings.

the magnetic stiffness k =12,990 N/m and the damping coefficient c =4.5 Ns/m are obtained using curve fitting method.

B. Rotor model

Fig.4 shows the rotor models (Model-1, 2 and 3) supported by two kinds of bearings (SMB and pivot bearing). The rotor Model-1 (Length: 192 mm), rotor Model-2 (Length: 232 mm) and rotor Model-3 (Length: 232 mm) are supported by (a) a SMB and a pivot bearing, (b) two SMBs and a pivot bearing and (c) two SMBs, respectively. The magnetic stiffness k and damping coefficient c are obtained using impulse responses for the rotor. The pivot bearing is composed of a small stainless bar (D3 mm ×L5 mm), which is attached to the rotor bottom.

C. Simulation

By using the rotor models shown in Fig.4, the rotor analysis (finite element method) is performed. In the simulation, the rotor spins up to a speed of 20,000 rpm. Then, the displacements for three models are analyzed. Fig.5 shows the relationships between rotor displacement and rotation speed for (a) rotor Model-1, (b) rotor Model-2 and (c) rotor Model-3. The displacements in Fig.5(a) are analyzed near the points of pivot bearing, turbine blade and SMB. From the result in

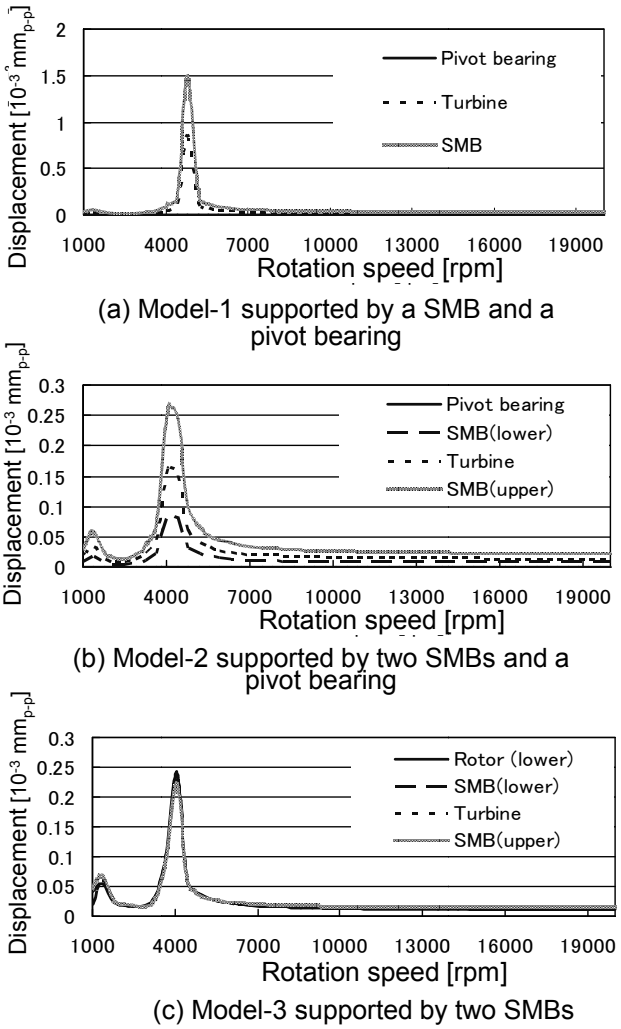

Fig. 5. Rotor displacements for three models 1-3.

Fig.5(a), each displacement is relatively small over a rotation speed range except for a speed of ≈5,000 rpm. From the result in Fig.5(b), each displacement is very small (smaller than 0.03 x10^{-3} mm) over a rotation speed range except for a speed of ≈4,000 rpm. From the

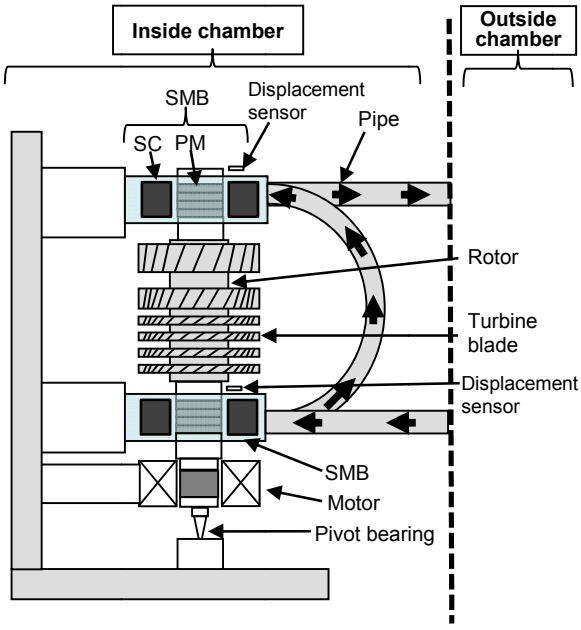

Fig. 6. Schematic illustration of the experimental setup.

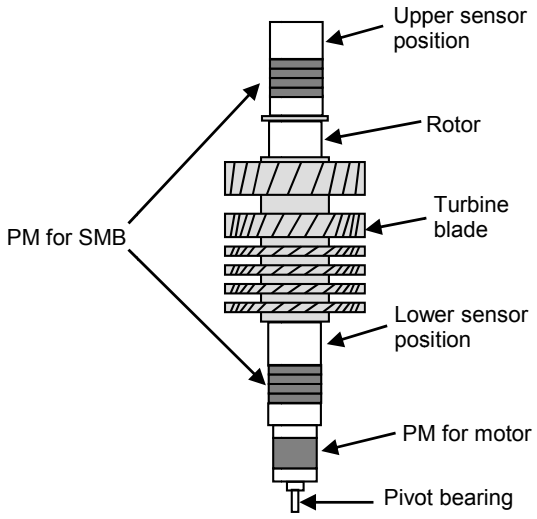

Fig. 7. Schematic illustration of the developed rotor.

result in Fig.5(c), each displacement is very small (smaller than 0.02 x10^{-3} mm) over a rotation speed range except for a speed of ≈4,000 rpm. Hereafter, the rotor Model-2 and Model-3 are adopted in our study because of the small displacements.

III. Experimental Setup

Fig.6 shows a schematic illustration of the experimental setup composed of a rotor with turbine blades, two SMBs, a pivot bearing, a PM motor and two eddy current displacement sensors. The SMB is composed of the same doughnut- shaped superconductor

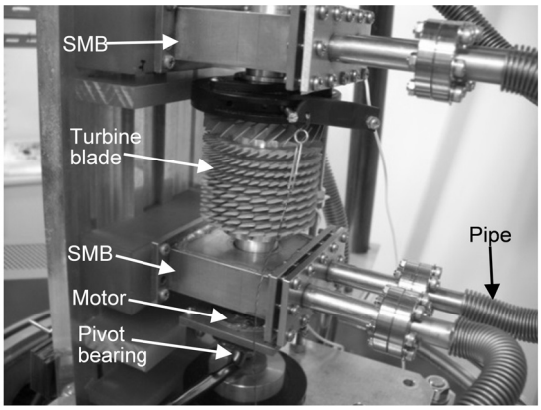

Fig. 8. Photo of the experimental setup of turbo molecular pump.

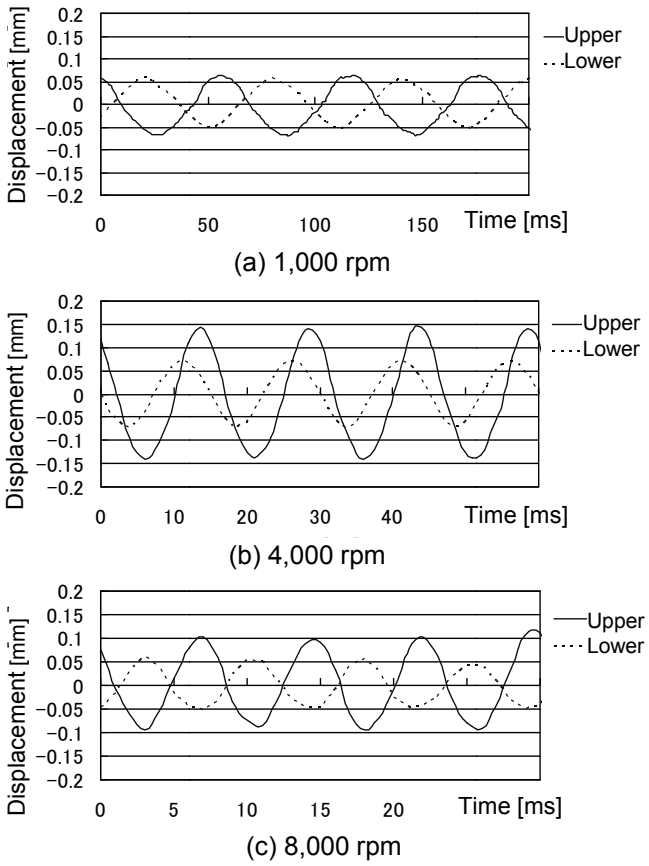

Fig. 9. Experimental results of rotor displacements for the rotor Model-2.

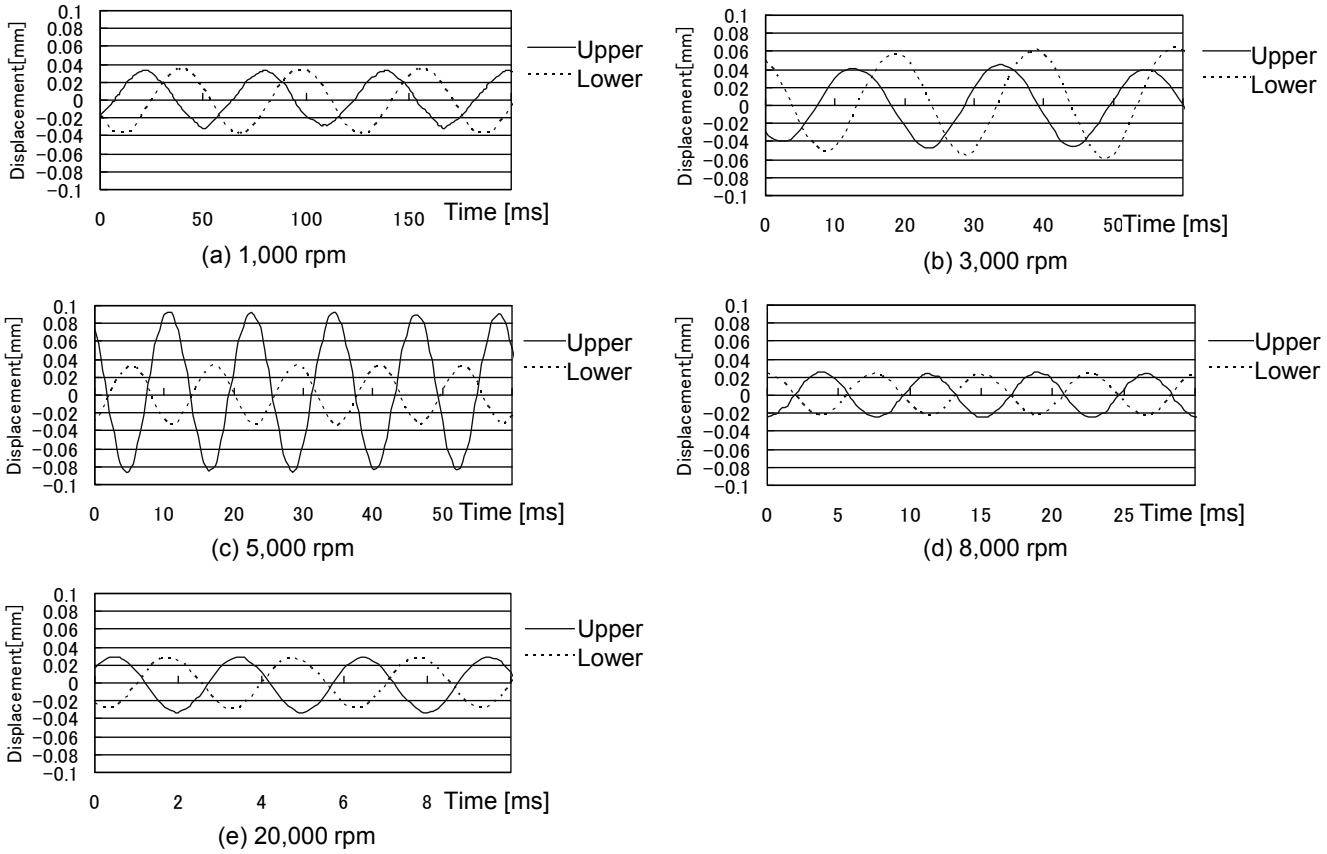

Fig. 10. Experimental results of rotor displacements for the rotor Model-3.

and the same four PMs as those mentioned in Figs.2 and 3. Fig.7 shows the schematic illustration of the developed rotor. The rotor is composed of turbine blades, PMs for SMB and a pivot for bearing, and measures 590g in weight. The rotor structure of Model-2 is basically the same as the rotor Model-3. Fig.8 shows the photo of the experimental setup. Each part in Fig.8 is corresponding to that in Fig.6.

IV. Experimental Results and Discussions

Fig.9 shows the experimental results of rotor displacements for the rotor Model-2, representing the displacements at speeds of (a) 1,000, (b) 4,000 and (c) 8,000 rpm. The solid lines and dotted lines represent the rotor displacement at the upper part and the lower part, respectively. At a low speed of 1,000 rpm, the displacement amplitude is less than $\cong 0.07$ mm as shown in Fig.9(a). At a higher speed of 8,000 rpm, the displacement amplitude is less than $\cong 0.1$ mm as shown in Fig.9(c). On the other hand, the displacement amplitude at a speed of 4,000 rpm is $\cong 0.15$ mm, which corresponds to the resonance speed. The resonance rotation speed is almost equal to the simulation result in Fig.5(b). Just after the rotor increases the speed higher than 8,000 rpm, the rotor suddenly stops the rotation because of mechanical contacts with the SMB stator.

Fig.10 shows the experimental results of rotor displacements for the rotor Model-3, representing the displacements at speeds of (a) 1,000, (b) 3,000, (c) 5,000, (d) 8,000 and (c) 20,000 rpm. The solid lines and dotted lines represent the rotor displacement at the upper part and the lower part, respectively. At low speeds of 1,000 and 3,000 rpm, the displacement amplitudes are less than $\cong 0.04$ mm as shown in Figs.9(a) and (b). At higher speeds of 8,000 and 20,000 rpm, the displacement amplitudes are less than $\cong 0.03$ mm as shown in Figs.9(d) and (e). On the other hand, the displacement amplitude at a speed of 5,000 rpm is $\cong 0.09$ mm, which corresponds to the resonance rotation speed. The resonance rotation speed is almost equal to the simulation result in Fig.5(c). We cannot increase the rotor speed higher than 20,000 rpm because of the PM motor performance.

From the experimental results, the rotor Model-3 with two SMBs is better than the rotor Model-2 with two

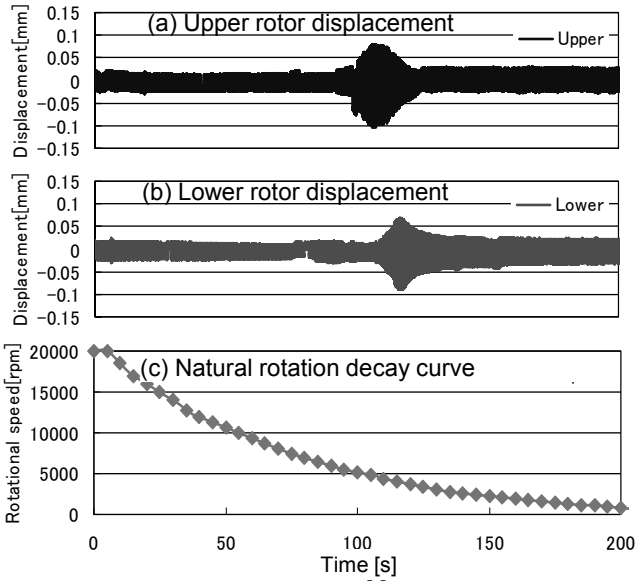

Fig. 11. Experimental results of free-run test for the rotor Model-3.

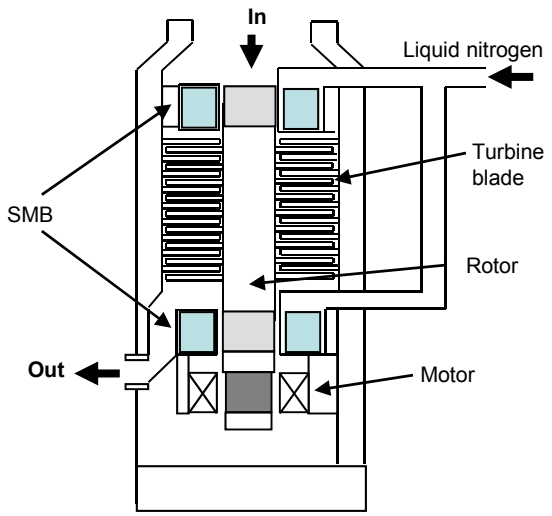

Fig.12. Image of turbo molecular pump using two SMBs.

SMBs and a pivot bearing. Hereafter, the rotor Model-3 with two SMBs is adopted in our study.

Thus, spin down tests are performed using the rotor Model-3. Fig.11 shows one of the experimental results of free-run test for the rotor Model-3, representing (a) upper rotor displacement, (b) lower rotor displacement and (c) natural rotation decay curve. Figs.10(a) and (b) show that the displacement amplitudes are smaller than $\cong 0.04$ mm over a wide time range except for rotation speeds between 4,000 and 5,000 rpm.

Fig.12 shows an image of turbo molecular pump composed of a rotor with two SMBs, turbine blades and a permanent magnet (PM) motor. The pump has a gas inlet at the top and a gas outlet at the lower side. Usually, the gas inlet is connected to a vacuum chamber using a vacuum hose to exhaust the chamber to a certain degree of vacuum. At the same time, water molecules in the air are trapped on the SMB surface and the turbine blades surface. This is called “trapping effect”. Thus, the turbo molecular pump with SMBs has some higher performances than conventional turbo molecular pumps because water molecules are easily trapped by trapping effect.

V. Summary

In this study, the rotor Model-1, 2 and 3 supported by two kinds of bearings (SMB and pivot bearing) are proposed. From the simulation results, the rotor Model-2 and Model-3 are adopted out of the three models because of the small displacements. From some experimental results, it is found that the displacement amplitudes of the rotor Model-3 are a little smaller than those of the rotor Model-2 over a wide rotation speed range.

References

[1] G. F. Weston, Ultrahigh vacuum practice, Butterworths, 1985.
[2] S. Jayaram and E. Gonzalez, Design and construction of a low-cost economical thermal vacuum chamber for spacecraft environmental testing, Journal of Engineering, Design and Technology, vol. 9, no.1, pp.47- 62, 2011.
[3] M. Komori, A. Tsuruta, S. Fukata and T. Matsushita : A new type of superconducting bearing system using high Tc superconductors and dynamics, Applied Superconductivity, vol.2, no.7/8, pp.499-509, 1995.
[4] K. Murakami, M. Komori and H. Mitsuda, Flywheel Energy Storage System Using SMB and PMB, IEEE Trans. on Applied Superconductivity, vol. 17, no. 2, pp. 2146-2149, June 2007
[5] Mochimitsu Komori, Bunpei Nakaya, Ken-ichi Asami, Nobuo Sakai, Magnetically levitated conveyer using high Tc superconducting levitation and its evaluations, Journal of The Japan Society of Applied Electromagnetics and Mechanics, Vol. 20, No. 2, pp. 520-525, July 201